Eur. Phys. J. A **21**, 313–321 (2004)
DOI 10.1140/epja/i2003-10203-3

THE EUROPEAN PHYSICAL JOURNAL A

Analysis of the Λp final-state interaction in the reaction p + p → K⁺(Λp)

F. Hinterberger[1,a] and A. Sibirtsev[2,3]

[1] Helmholtz-Institut für Strahlen- und Kernphysik, Universität Bonn, Nußallee 14-16, D-53115, Bonn, Germany
[2] Institut für Kernphysik, Forschungszentrum Jülich, D-52425 Jülich, Germany
[3] Special Research Center for the Subatomic Structure of Matter (CSSM) and Department of Physics and Mathematical Physics, University of Adelaide, SA 5005, Australia

Received: 19 December 2003 / Revised version: 8 January 2004 /
Published online: 17 August 2004 –
Communicated by V. Vento

Abstract. The missing-mass spectrum measured in high-resolution studies of the reaction $pp \to K^+X$ is analyzed with respect to the strong final-state interaction near the Λp production threshold. The observed spectrum can be described by factorizing the reaction amplitude in terms of a production amplitude and a final-state scattering amplitude. Parametrizing the Λp final-state interaction in terms of the inverse Jost function allows a direct extraction of the low-energy phase-equivalent potential parameters. Constraints on the singlet and triplet scattering lengths and effective ranges are deduced in a simultaneous fit of the Λp invariant-mass spectrum and the total-cross-section data of the free Λp scattering using the effective-range approximation.

PACS. 13.75.Ev Hyperon-nucleon interactions – 21.30.Fe Forces in hadronic systems and effective interactions – 24.10.-i Nuclear reaction models and methods – 25.40.-h Nucleon-induced reactions

1 Introduction

Experimental information on the Λp interaction has been derived from the analysis of hypernuclei, Λp scattering experiments and studies of the Λp final-state interaction (FSI) in strangeness transfer reactions. The binding energy of light hypernuclei shows that the low-energy Λp interaction is attractive. In addition, the Λp interaction is spin-dependent and the singlet interaction is stronger than the triplet one [1–3]. The free Λp scattering was studied in bubble chamber measurements [4–6]. In the low-momentum region the elastic cross-sections were analyzed in terms of the S-wave singlet and triplet scattering lengths and effective ranges. However, these determinations are characterized by large variances and covariances since the data only support the determination of a spin-averaged scattering length and effective range [6].

The strong effect due to the Λp FSI was observed in strangeness transfer reactions [7–9] and and in associated strangeness production reactions [10–16]. The Λp production in the $K^-d \to \pi^-\Lambda p$, $\pi^+d \to K^+\Lambda p$, $\gamma d \to K^0\Lambda p$ and $pp \to K^+\Lambda p$ reactions can provide substantial improvement in an evaluation of the low-energy Λp scattering.

Intensive theoretical studies of the hyperon-nucleon interaction with the Nijmegen [17–20] and Jülich [21–23] potential models predict the hyperon-nucleon potentials and phase shift parameters. These models also predict the singlet and triplet scattering length and effective-range parameters of the free S-wave Λp interaction.

The present paper refers to the associated strangeness reaction $pp \to K^+(\Lambda p)$ which is characterized by a strong FSI near the Λp production threshold. In most experiments the Λp system was measured inclusively. Exclusive measurements of the $pp \to K^+\Lambda p$ reaction were performed at COSY [14,15] and SATURNE [16]. Theoretical analyses of the reactions were done [24–37] by applying the meson exchange model and including the Λp FSI generally modelled by Nijmegen or Jülich potentials.

The aim of the present paper is to perform an analysis of the Λp FSI in the reaction $pp \to K^+(\Lambda p)$ and an evaluation of the Λp low-energy interaction parameters. Using the Watson-Migdal approximation [38–41] the reaction amplitude is factorized in terms of a production matrix element and a FSI enhancement factor, which can be represented by the inverse Jost function [42–45]. We analyze experimental results from SATURNE collected by Siebert *et al.* [13], which are characterized by a high statistical accuracy and a high invariant-mass resolution. Furthermore, in the fitting procedure the missing-mass resolution

[a] e-mail: fh@iskp.uni-bonn.de

is taken into account by folding the theoretical expressions with the experimental resolution function.

The analysis shows that the shape of the sharply rising invariant-mass spectrum depends strongly on the singlet and triplet scattering length and effective-range parameters. But only two parameters, the spin-averaged scattering length and effective-range parameters, can be deduced within an acceptable confidence level by fitting the Λp missing-mass spectrum. Additional information can be obtained by taking the total-cross-section data for the free Λp scattering into account and including these data in an overall fit. At low energies the total cross-section can be described in a model-independent way using the effective-range approximation [46–48]. Thus, by fitting simultaneously the Λp invariant-mass spectrum and the available total cross-section data of the free Λp scattering severe constraints on the singlet and triplet scattering length and effective-range parameters can be deduced. This method allows also to test theoretical model predictions.

2 The formalism

2.1 Phase space distribution

The $pp \to K^+\Lambda p$ double differential cross-section is given as

$$\frac{\mathrm{d}^2\sigma}{\mathrm{d}\Omega_K \mathrm{d}M_{\Lambda p}} = |\tilde{\mathcal{M}}|^2 \, \Phi_3, \tag{1}$$

where $\tilde{\mathcal{M}}$ is the Lorentz-invariant reaction amplitude and the three-body phase space distribution function is

$$\Phi_3 = \frac{\pi}{16(2\pi)^5} \frac{p_K^2 q}{p_p m_p [(E_p + m_p)p_K - E_K p_p \cos\theta_K]}, \tag{2}$$

where q is the momentum of Λ in the Gottfried-Jackson rest-frame of the produced two-particle subsystem $X = \Lambda + p$, $M_{\Lambda p}$ is the corresponding invariant mass and p_p, E_p, p_K, E_K, θ_K, Ω_K are defined in the laboratory system. Obviously, in inclusive measurements the invariant mass $M_{\Lambda p}$ is equal to the missing mass M_X below the Σ-hyperon production threshold. Equation (2) is consistent with the kinematical definitions of refs. [49,50].

2.2 Final-state interaction

In the Watson-Migdal approximation [38–40] the FSI is taken into account by introducing a FSI enhancement factor $|C_{\mathrm{FSI}}|^2$,

$$\frac{\mathrm{d}^2\sigma}{\mathrm{d}\Omega_K \mathrm{d}M_{\Lambda p}} = |\mathcal{M}|^2 \, |C_{\mathrm{FSI}}|^2 \, \Phi_3, \tag{3}$$

where now $\mathcal{M}$ is a pure production matrix element and the FSI amplitude C_{FSI} depends on the internal momentum q of the Λp subsystem. It converges to 1 for $q \to \infty$ where the S-wave FSI enhancement vanishes.

Applying the factorization we assume that the production operator $\mathcal{M}$ is constant, *i.e.* does not depend on the internal kinetic energy of the Λp subsystem. In case of the $pp \to K^+\Lambda p$ reaction this assumption is supported by the kinematics which provides a focus onto the Λp FSI. The internal kinetic energy of the Λp subsystem is almost zero near the Λp threshold, whereas the $K^+\Lambda$ and K^+p subsystems have large internal kinetic energies. Even if the $pp \to K^+\Lambda p$ reaction is dominated [29–32] by intermediate baryonic resonances coupled to the $K^+\Lambda$ system a small variation of the invariant Λp mass does practically not affect the production amplitude.

The methods for studying the FSI between the particles have been developed in different areas of physics, ranging from atomic physics to high-energy particle physics [41]. Taking the inverse Jost function [42,43] the correction due to the FSI is given as

$$C_{\mathrm{FSI}} = \frac{q - i\beta}{q + i\alpha}, \qquad |C_{\mathrm{FSI}}|^2 = \frac{q^2 + \beta^2}{q^2 + \alpha^2}. \tag{4}$$

The potential parameters α and β can be used to establish phase-equivalent Bargmann potentials [44,45]. They are related to the scattering lengths a, and effective ranges r of the low-energy S-wave scattering

$$\alpha = \frac{1}{r}\left(1 - \sqrt{1 - 2\frac{r}{a}}\right), \quad \beta = \frac{1}{r}\left(1 + \sqrt{1 - 2\frac{r}{a}}\right). \tag{5}$$

The Λp system can couple to singlet ${}^1S_0$ and triplet ${}^3S_1$ states. Near production threshold the singlet-triplet transitions due to the final-state interaction cannot occur. Therefore, the contributions of the spin-singlet and spin-triplet final states can be added incoherently. Taking the spin-statistical weights into account the unpolarized double differential cross-section may be written as

$$\frac{\mathrm{d}^2\sigma}{\mathrm{d}\Omega_K \mathrm{d}M_{\Lambda p}} = \Phi_3 \left[0.25 \, |\mathcal{M}_s|^2 \, \frac{q^2 + \beta_s^2}{q^2 + \alpha_s^2} + \; 0.75 \, |\mathcal{M}_t|^2 \, \frac{q^2 + \beta_t^2}{q^2 + \alpha_t^2} \right]. \tag{6}$$

This equation leaves six free parameters, the singlet and triplet potential parameters α_s, β_s, α_t, β_t and the production matrix elements $|\mathcal{M}_s|$ and $|\mathcal{M}_t|$. Instead of the parameters α_s, β_s, α_t and β_t one can equally well use the singlet and triplet scattering length and effective-range parameters a_s, r_s, a_t and r_t. The functional dependence on the invariant mass $M_{\Lambda p}$ can be evaluated by inserting the corresponding expression for the internal momentum q of the Λp system,

$$q = \frac{\sqrt{M_{\Lambda p}^2 - (m_\Lambda + m_p)^2}\sqrt{M_{\Lambda p}^2 - (m_\Lambda - m_p)^2}}{2M_{\Lambda p}}. \tag{7}$$

2.3 Missing-mass resolution

The theoretical missing-mass spectrum of eq. (6) has to be folded with the missing-mass resolution function before

comparing with the data. Introducing the missing-mass resolution function $g(\tilde{M}_{\Lambda p} - M_{\Lambda p})$ and denoting the r.h.s. of eq. (6) by $f_0(M_{\Lambda p})$ yields the distribution function $f(M_{\Lambda p})$ which has to be compared with the data,

$$f(M_{\Lambda p}) = \int f_0(\tilde{M}_{\Lambda p})\, g(\tilde{M}_{\Lambda p} - M_{\Lambda p})\, \mathrm{d}\tilde{M}_{\Lambda p}\,, \qquad (8)$$

where the resolution function is given as

$$g(\tilde{M}_{\Lambda p} - M_{\Lambda p}) = \frac{1}{\sqrt{2\pi}} \frac{1}{\sigma_M} \exp - \frac{(\tilde{M}_{\Lambda p} - M_{\Lambda p} + \Delta M_{\Lambda p})^2}{2\sigma_M^2}. \qquad (9)$$

Here, σ_M denotes the one-standard-deviation width and the shift $\Delta M_{\Lambda p}$ takes a systematic calibration error of the invariant-mass scale into account. For the comparison with the SATURNE data the values $\Delta M_{\Lambda p} = 1.7$ MeV and $\sigma_M = 2.0$ MeV [13] are used.

2.4 The Λp cross-section

In the effective-range approximation [46–48] the total cross-section of the free Λp elastic scattering can be expressed in terms of the singlet and triplet scattering length and effective-range parameters a_s, a_t, r_s and r_t,

$$\sigma_{\Lambda p} = \frac{\pi}{q^2 + \left(-\frac{1}{a_s} + \frac{r_s q^2}{2}\right)^2} + \frac{3\pi}{q^2 + \left(-\frac{1}{a_t} + \frac{r_t q^2}{2}\right)^2}. \qquad (10)$$

Here, q is the c.m. momentum of the Λp scattering. This equation can be applied at low energies where S-wave contributions dominate.

3 The results of the fits

The program Minuit of the CERN program library [51] was used in order to perform nonlinear least-square fits. We fit the experimental results [13] for the missing-mass spectrum from the $pp \to K^+X$ reaction measured at proton beam energy $T_p = 2.3$ GeV and kaon emission angle of $\theta_K = 10.3°$ using eqs. (6) and (8), respectively. We fit the strong FSI enhancement near the Λp threshold assuming that the S-wave FSI is dominant. Therefore, we take only data corresponding to very low c.m. momenta q in the Λp system. The fits include 29 experimental points of the missing-mass spectrum from the Λp threshold at 2054 MeV up to the invariant mass of the Λp system of 2095 MeV. This $M_{\Lambda p}$ range corresponds to c.m. momenta q in the Λp system between 0 and 200 MeV/c.

Low-energy total Λp cross-section data from bubble chamber measurements [4–6] are fitted simultaneously using eq. (10). The fits include 12 total Λp cross-section data points covering c.m. momentum range $60 \le q \le 135$ MeV/c.

It is worthwhile to mention that the $pp \to K^+X$ reaction provides high-quality data even at very small q near the Λp threshold, whereas $\Lambda p \to \Lambda p$ data are available only for $q \ge 60$ MeV/c. Also the number of data and the accuracy of the $pp \to K^+X$ measurement is substantially higher. Therefore it is very attractive to include the $pp \to K^+X$ data in the evaluation of the low-energy phase-equivalent potential parameters as far as the evaluation remains model independent.

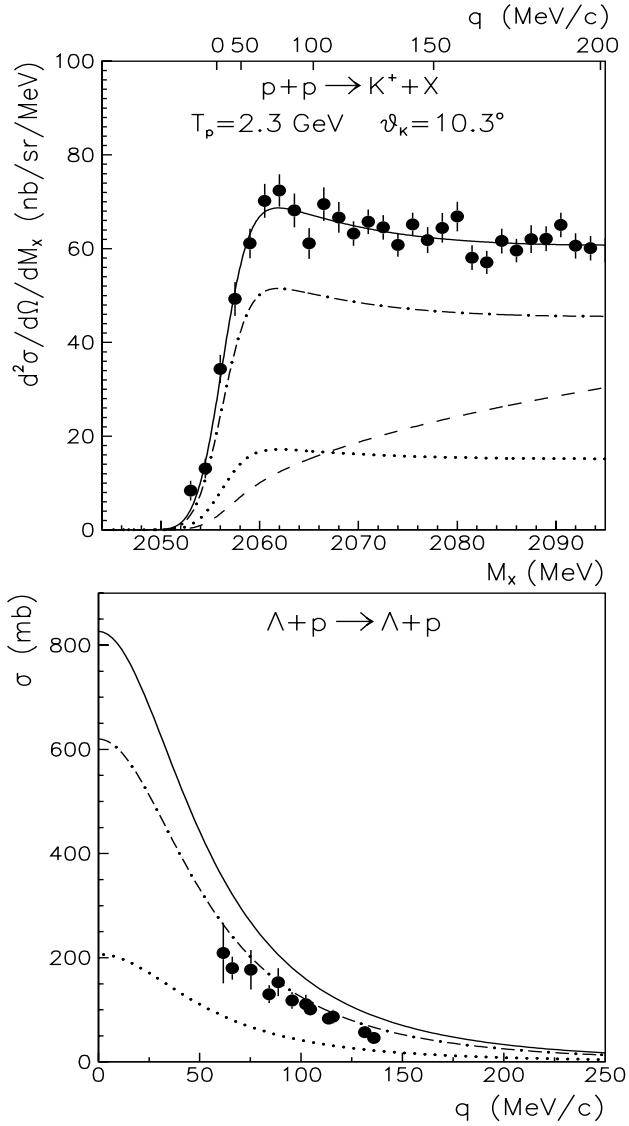

Fig. 1. Top: missing-mass spectrum of the reaction $pp \to K^+X$ measured at $T_p = 2.3$ GeV and $\theta_K = 10.3°$ [13]. The upper axis indicates the c.m. momentum q of the Λp system. Bottom: total Λp cross-section [4–6] as a function of the c.m. momentum q. Solid lines: fit curves with parameters given by eq. (11) from a three-parameter fit of the missing-mass spectrum alone, dashed line: phase space distribution, dotted lines: singlet contributions, dash-dotted lines: triplet contributions.

The quality of the least-square fits is given by total χ^2 and reduced χ^2/n.d.f. where n.d.f. is the number of degrees of freedom given by the number of data minus the number of the fit parameter. In calculating the parameter errors nonlinearities and parameter correlations were taken into account. The error for a given parameter is

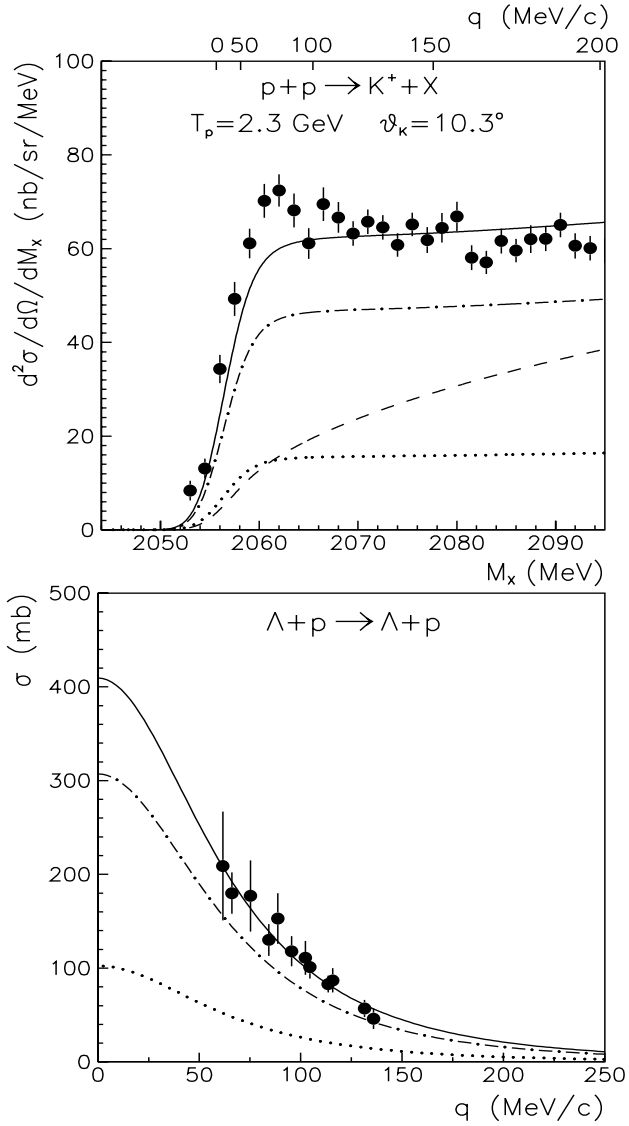

Fig. 2. Same as in fig. 1. Solid lines: Fit curves with $\bar{a}$ and $\bar{r}$ given by eq. (12) from a two-parameter fit of the total-cross-section data alone and $|\bar{\mathcal{M}}|^2$ given by eq. (13), dashed line: phase space distribution, dotted lines: singlet contributions, dash-dotted lines: triplet contributions.

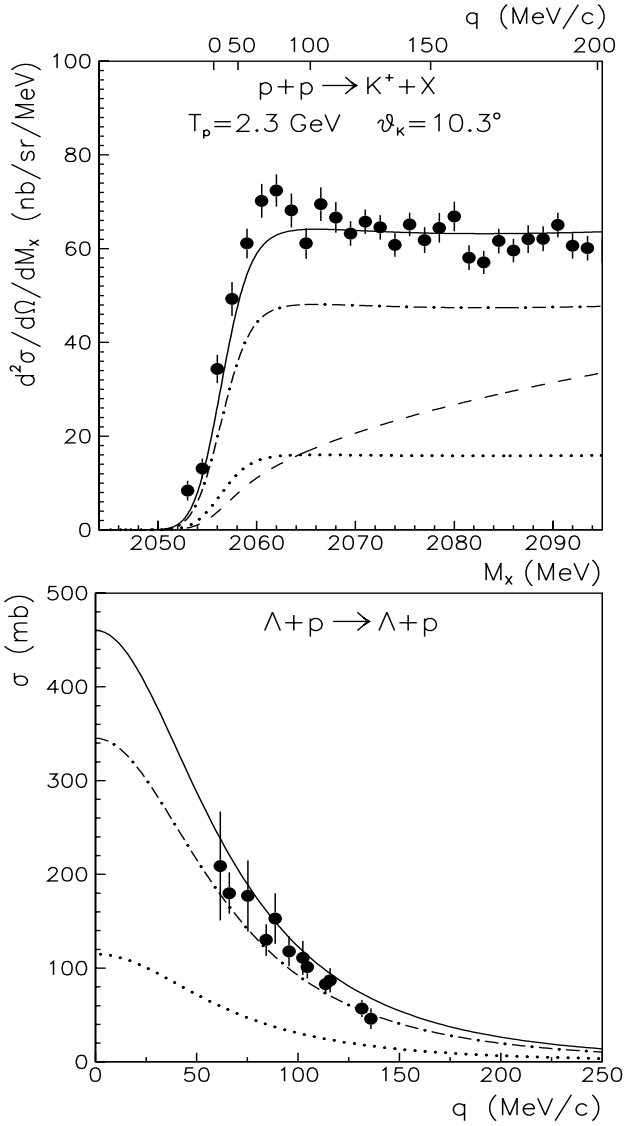

Fig. 3. Same as in fig. 1. Solid lines: Fit curves with parameters given by eq. (14) from a combined three-parameter fit of the missing-mass spectrum and the total-cross-section data, dashed line: phase space distribution, dotted lines: singlet contributions, dash-dotted lines: triplet contributions.

defined as the change of that parameter which causes χ^2 to increase by one while re-fitting all other free parameters. Due to the nonlinearities the resulting error intervals are in general asymmetric.

3.1 Three-parameter fit

In a three-parameter fit we determine spin-averaged parameters by applying the constraints

$$|\mathcal{M}_s|^2 = |\mathcal{M}_t|^2 = |\bar{\mathcal{M}}|^2, \quad a_s = a_t = \bar{a}, \quad r_s = r_t = \bar{r}\,.$$

The three-parameter fit yields the production matrix element squared $|\bar{\mathcal{M}}|^2$ and the spin-averaged scattering length $\bar{a}$ and effective range $\bar{r}$.

In a first step we fit only the missing-mass spectrum without taking the Λp total-cross-section data into account. The three-parameter fit yields an excellent description of the missing-mass spectrum but fails completely to reproduce the total-cross-section data (χ^2/n.d.f. = 18.0, see fig. 1). The fit parameters of the missing-mass spectrum are

$$|\bar{\mathcal{M}}|^2 = 15.4^{+1.5}_{-1.6}\ \text{b/sr}, \quad \chi^2/\text{n.d.f.} = 0.98,$$
$$\bar{a} = -2.57^{+0.20}_{-0.23}\ \text{fm}, \quad \bar{r} = 2.47^{+0.23}_{-0.24}\ \text{fm}. \qquad (11)$$

The dotted and dashed-dotted lines in fig. 1 and in the following figs. 2-4 show the corresponding singlet and triplet contributions. The dashed lines show the phase space distributions without the FSI enhancement factor, *i.e.* $(0.25|\mathcal{M}_s|^2 + 0.75|\mathcal{M}_t|^2)\Phi_3$.

Table 1. Five-parameter fit results for a_s, r_s, a_t, r_t and $|\mathcal{M}_s|^2$ and different ratios $|\mathcal{M}_t|^2/|\mathcal{M}_s|^2$ of the triplet and singlet production matrix elements.

$\lvert\mathcal{M}_t\rvert^2/\lvert\mathcal{M}_s\rvert^2$	$\lvert\mathcal{M}_s\rvert^2$ (b/sr)	a_s (fm)	r_s (fm)	a_t (fm)	r_t (fm)	χ^2	χ^2/n.d.f.
0.00	$61.4^{+5.9}_{-6.3}$	$-2.6^{+0.2}_{-0.2}$	$2.47^{+0.23}_{-0.24}$	$-1.5^{+0.2}_{-0.3}$	$3.6^{+0.9}_{-0.9}$	29.0	0.805
0.10	$46.7^{+4.2}_{-4.5}$	$-2.7^{+0.3}_{-0.4}$	$2.25^{+0.23}_{-0.24}$	$-1.5^{+0.3}_{-0.3}$	$3.8^{+1.0}_{-1.0}$	29.0	0.807
0.25	$34.4^{+3.0}_{-3.2}$	$-2.9^{+0.3}_{-0.5}$	$1.97^{+0.22}_{-0.23}$	$-1.4^{+0.3}_{-0.4}$	$4.0^{+1.1}_{-1.2}$	29.1	0.809
0.50	$24.0^{+2.1}_{-2.3}$	$-3.1^{+0.4}_{-0.6}$	$1.63^{+0.18}_{-0.19}$	$-1.3^{+0.4}_{-0.4}$	$4.5^{+1.3}_{-1.3}$	29.2	0.812
1.00	$15.0^{+1.4}_{-1.6}$	$-3.2^{+0.4}_{-0.6}$	$1.25^{+0.13}_{-0.15}$	$-1.3^{+0.4}_{-0.5}$	$5.4^{+1.6}_{-1.}$	29.4	0.816
2.00	$8.7^{+0.8}_{-1.0}$	$-3.3^{+0.4}_{-0.6}$	$0.90^{+0.09}_{-0.10}$	$-1.2^{+0.5}_{-0.6}$	$6.5^{+2.0}_{-2.1}$	29.6	0.821
4.00	$4.7^{+0.4}_{-0.5}$	$-3.3^{+0.4}_{-0.6}$	$0.63^{+0.06}_{-0.07}$	$-1.2^{+0.5}_{-0.8}$	$7.8^{+2.7}_{-2.7}$	29.8	0.827
8.00	$2.4^{+0.2}_{-0.2}$	$-3.4^{+0.4}_{-0.6}$	$0.44^{+0.04}_{-0.05}$	$-1.2^{+0.6}_{-1.0}$	$9.2^{+3.5}_{-3.5}$	29.9	0.832

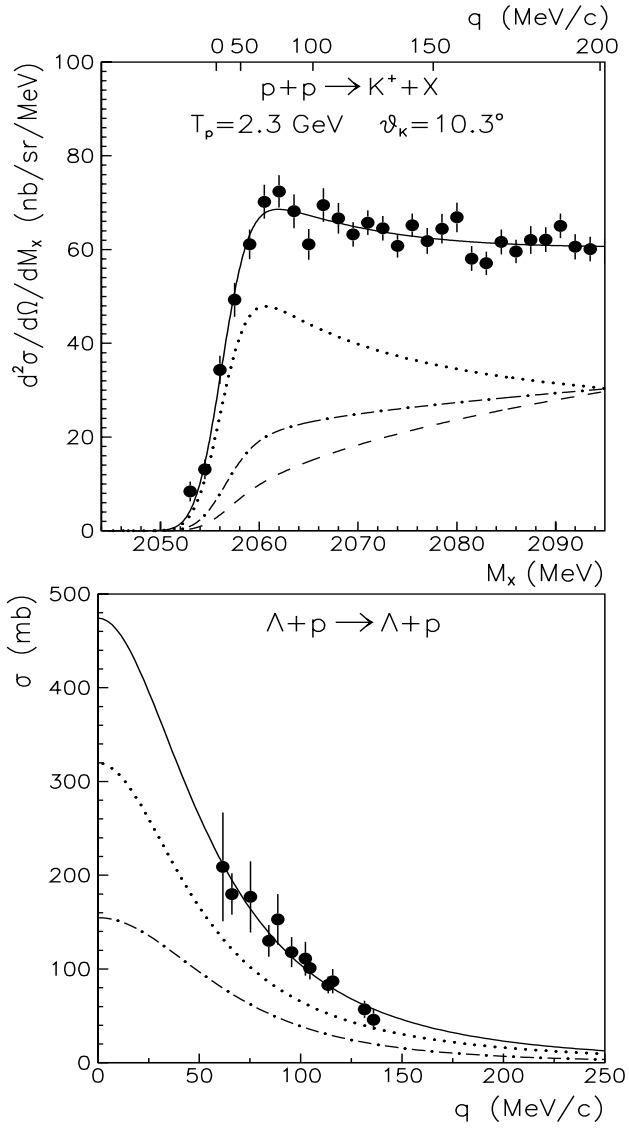

Fig. 4. Same as in fig. 1. Solid lines: Fit curves with parameters given by eq. (15) from a combined five-parameter fit of the missing-mass spectrum and the total-cross-section data, dashed line: phase space distribution, dotted lines: singlet contributions, dash-dotted lines: triplet contributions.

Vice versa, we take only the total-cross-section data into account and determine $\bar{a}$ and $\bar{r}$ in a two-parameter fit. The resulting fit parameters are

$$\bar{a} = -1.81^{+0.18}_{-0.21}\ \text{fm},\ \ \bar{r} = 3.24^{+0.48}_{-0.48}\ \text{fm},\ \ \chi^2/\text{n.d.f.} = 0.39. \tag{12}$$

Taking those parameters fixed and fitting only $|\bar{\mathcal{M}}|^2$ yields for the missing-mass spectrum

$$|\bar{\mathcal{M}}|^2 = 19.5^{+0.2}_{-0.2}\ \text{b/sr}, \quad \chi^2/\text{n.d.f.} = 3.7. \tag{13}$$

This procedure yields an excellent fit of the total-cross-section data but fails completely to describe the missing-mass spectrum (see fig. 2).

In a next step, we determine spin-averaged parameters in a combined fit, *i.e.* by fitting simultaneously the missing-mass spectrum and the total-cross-section data. The resulting parameters are

$$|\bar{\mathcal{M}}|^2 = 16.9^{+1.2}_{-1.2}\ \text{b/sr}, \quad \chi^2/\text{n.d.f.} = 2.2,$$
$$\bar{a} = -1.91^{+0.10}_{-0.11}\ \text{fm}, \quad \bar{r} = 2.74^{+0.20}_{-0.20}\ \text{fm}. \tag{14}$$

This procedure fails to describe both the missing-mass spectrum and the total-cross-section data (see fig. 3). This failure is a direct indication that the spin dependence of the Λp interaction must be taken into account.

3.2 Five-parameter fit

Now the data on the total Λp cross-section and $pp \to K^+X$ missing-mass spectrum are fitted in a combined fit with the singlet and triplet scattering lengths and effective ranges a_s, r_s, a_t, r_t as separate free parameters. Taking the unknown quantities $|\mathcal{M}_s|^2$ and $|\mathcal{M}_t|^2$ into account a six-parameter fit should be performed. However, it turned out that the χ^2 criterion cannot be used to determine simultaneously $|\mathcal{M}_s|^2$ and $|\mathcal{M}_t|^2$. This is due to the fact that the resulting χ^2 depends only weakly on the ratio $|\mathcal{M}_t|^2/|\mathcal{M}_s|^2$ as is indicated in table 1. Therefore, five-parameter fits were performed taking $|\mathcal{M}_s|^2$ as free parameter and the ratio $|\mathcal{M}_t|^2/|\mathcal{M}_s|^2$ as fixed parameter. By this method valuable constraints on the singlet and triplet scattering lengths and effective ranges can be deduced from the data.

Table 2. Test of potential model results performed with two-parameter fit.

Model	a_s (fm)	r_s (fm)	a_t (fm)	r_t (fm)	$\|\mathcal{M}_s\|^2$ (b/sr)	$\|\mathcal{M}_t\|^2$ (b/sr)	χ^2	χ^2/n.d.f.
Nijm a	−0.71	5.86	−2.18	2.76	$0. \pm 0.1$	22.8 ± 0.2	47.6	1.22
Nijm b	−0.90	4.92	−2.13	2.84	$0. \pm 0.1$	23.4 ± 0.2	53.9	1.38
Nijm c	−1.20	4.11	−2.08	2.92	$0. \pm 0.1$	23.9 ± 0.2	62.2	1.60
Nijm d	−1.71	3.46	−1.95	3.08	$0. \pm 0.1$	25.0 ± 0.2	83.3	2.14
Nijm e	−2.10	3.19	−1.86	3.19	77.5 ± 0.7	$0. \pm 0.1$	76.6	1.97
Nijm f	−2.51	3.03	−1.75	3.32	74.7 ± 0.7	$0. \pm 0.1$	44.8	1.15
Jül Ã	−2.04	0.64	−1.33	3.91	7.3 ± 0.5	7.8 ± 1.6	55.9	1.43
Jül B̃	−0.40	12.28	−2.12	2.57	$0. \pm 0.1$	21.3 ± 0.2	43.6	1.12
Jül A	−1.56	1.43	−1.59	3.16	33.8 ± 0.3	$0. \pm 0.1$	80.2	2.06
Jül B	−0.56	7.77	−1.91	2.43	$0. \pm 0.1$	20.1 ± 0.2	55.5	1.42
NSC	−2.78	2.88	−1.41	3.11	71.6 ± 0.7	$0. \pm 0.1$	32.8	0.84
Nijm D	−1.90	3.72	−1.96	3.24	$0. \pm 0.2$	26.1 ± 0.2	91.6	2.35
Nijm F	−2.29	3.17	−1.88	3.36	77.4 ± 0.7	$0. \pm 0.1$	62.6	1.61
Jül 03	−1.02	4.49	−1.89	2.57	$0. \pm 0.1$	21.3 ± 0.2	62.4	1.60

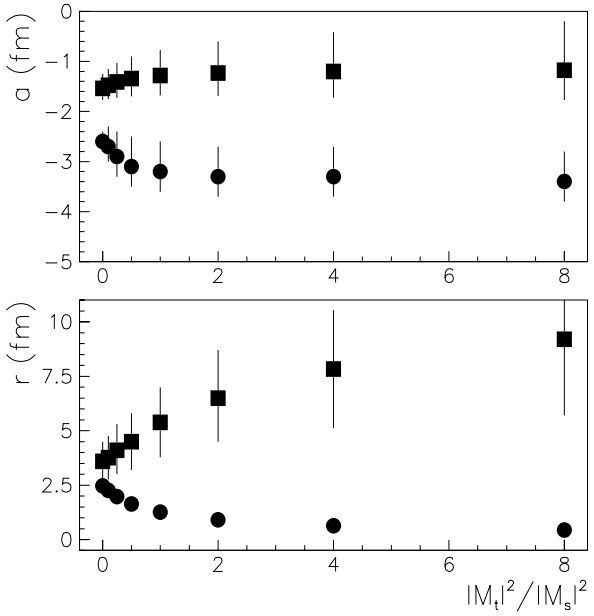

Fig. 5. The singlet (circles) and triplet (squares) scattering lengths and effective ranges as a function of the ratio $|\mathcal{M}_t|^2/|\mathcal{M}_s|^2$ resulting from the overall five-parameter fit to the total Λp cross-section and missing-mass spectrum measured in the $pp \to K^+X$ reaction.

It should be mentioned that the spin-statistical weights 0.25 and 0.75 of the singlet and triplet contributions have already been taken into account in the theoretical ansatz (6). Therefore the five-parameter search was started with the constraint $|\mathcal{M}_t|^2/|\mathcal{M}_s|^2 = 1$ yielding a solution with χ^2/n.d.f. = 0.82. The resulting parameters are

$$\begin{aligned} |\mathcal{M}_s|^2 &= 15.0^{+1.4}_{-1.6}\ \text{b/sr}, \quad \chi^2/\text{n.d.f.} = 0.82, \\ a_s &= -3.2^{+0.4}_{-0.6}\ \text{fm}, \quad r_s = 1.25^{+0.13}_{-0.15}\ \text{fm}, \\ a_t &= -1.3^{+0.4}_{-0.5}\ \text{fm}, \quad r_t = 5.4^{+1.6}_{-1.6}\ \text{fm}. \end{aligned} \tag{15}$$

Both the missing-mass spectrum and the total-cross-section data (see fig. 4) are perfectly reproduced. Then, the ratio $|\mathcal{M}_t|^2/|\mathcal{M}_s|^2$ was varied over a wide range of values and best-fit solutions of similar quality with χ^2/n.d.f. varying between 0.80 and 0.83 were found. The resulting fit parameters are listed in table 1 for $0 \le |\mathcal{M}_t|^2/|\mathcal{M}_s|^2 \le 8$.

A characteristic feature of the best-fit solutions is the fact that the singlet FSI enhancement factor at $q = 0$ is much larger than the triplet one, *e.g.* $\beta_s^2/\alpha_s^2 = 49.1$ and $\beta_t^2/\alpha_t^2 = 3.9$ for $|\mathcal{M}_t|^2/|\mathcal{M}_s|^2 = 1$. In spite of the statistical weight 0.25 the singlet contribution dominates the $pp \to K^+\Lambda p$ cross-section at $q = 0$, *e.g.* $0.25|\mathcal{M}_s|^2\beta_s^2/\alpha_s^2 = 183$ b/sr and $0.75|\mathcal{M}_t|^2\beta_t^2/\alpha_t^2 = 43.5$ b/sr for $|\mathcal{M}_t|^2/|\mathcal{M}_s|^2 = 1$. Solutions where the triplet contribution is larger than the singlet contribution do not fit the FSI enhancement of the missing-mass spectrum near $q = 0$ and can be excluded on the basis of the χ^2 criterion. This holds true even if one varies the ratio $|\mathcal{M}_t|^2/|\mathcal{M}_s|^2$ in a wide range.

The resulting best-fit parameters are shown in fig. 5 as a function of the ratio $|\mathcal{M}_t|^2/|\mathcal{M}_s|^2$. The variation of the ratio $|\mathcal{M}_t|^2/|\mathcal{M}_s|^2$ causes rather small variations of the parameters a_s, a_t and rather large variations of the parameters r_s, r_t, respectively. Therefore one can deduce important constraints on the singlet and triplet scattering lengths and effective ranges of the low-energy Λp interaction:

$$\begin{aligned} &-4.1\ \text{fm} < a_s < -2.3\ \text{fm}, \qquad r_s < 2.7\ \text{fm}, \\ &-1.8\ \text{fm} < a_t < -0.6\ \text{fm}, \qquad r_t > 2.7\ \text{fm}. \end{aligned} \tag{16}$$

4 Tests of potential model results

Available meson exchange potential model predictions of the S-wave Λp singlet and triplet scattering length and effective-range parameters are listed in table 2. Here the results from the Nijmegen model are denoted as Nijm D [17], Nijm F [18] and Nijm a-f [20]. The NSC

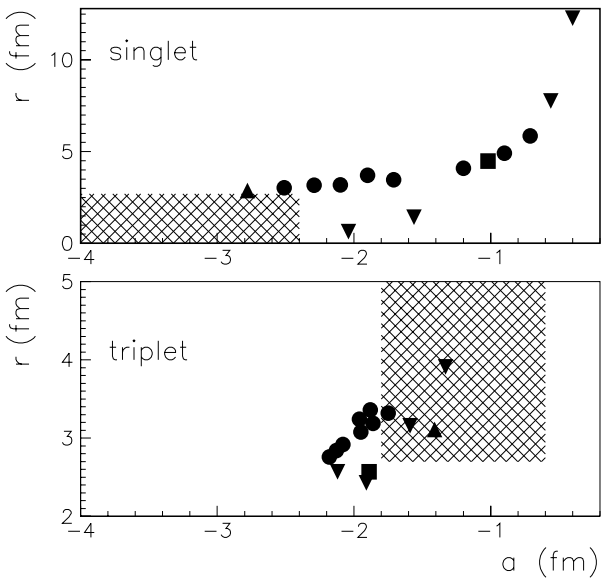

Fig. 6. Experimentally allowed regions (hatched rectangles) for Λp singlet and triplet scattering lengths and effective ranges, a_s, r_s and a_t, r_t deduced from five-parameter fits of the $pp \to K^+X$ missing-mass spectrum and the total Λp cross-section data. The symbols indicate theoretical results for singlet and triplet parameters from different models: Nijmegen [17,18] (circles), Jülich [22,21] (inverse triangles) and NSC [19] (triangle). The square shows most recent Jülich result [23].

parameters are taken from ref. [19]. The parameters given by Jülich model are denoted as Jül A, B [21] and Jül Ã, B̃ [22]. The most recent Jülich parameters are indicated as Jül 03 [23].

In fig. 6 the model predictions of a_s, r_s, a_t and r_t are compared with the five-parameter fit results of sect. 3. The experimentally allowed regions deduced from five-parameter fits are indicated by hatched rectangles. All model predictions of (a_s, r_s) and most predictions of (a_t, r_t) lie outside the experimentally allowed regions. In most cases the singlet scattering lengths a_s are too small and the triplet scattering lengths a_t are too large.

A more direct test of the model predictions can be performed using eqs. (6) and (10). Keeping the predicted parameters fixed and fitting only the two free parameters $|M_s|^2$ and $|M_t|^2$ the calculated cross-sections are compared with the $pp \to K^+X$ missing-mass spectrum as well as the total Λp cross-section data and the χ^2 are deduced (see table 2). Excepting the model Jül Ã this procedure yields either $|M_s|^2 = 0$ or $|M_t|^2 = 0$. This is due to the fact that the models predict either a dominating singlet or triplet FSI enhancement. The resulting values of χ^2 should be compared with the best-fit value $\chi^2 = 29.0$ obtained in direct five-parameter fits (see table 1). Excepting the result of the NSC model all χ^2 values are essentially larger than 29.0. They indicate that those model predictions fail to reproduce simultaneously the missing-mass spectrum and the total-cross-section data.

5 Summary and conclusions

We analyzed the high-resolution $pp \to K^+X$ data of Siebert *et al.* [13] with respect to the strong FSI near the Λp production threshold. The observed missing-mass spectrum was described by factorizing the reaction amplitude in terms of a production amplitude and FSI amplitude which was parametrized in terms of the inverse Jost function. It was found that a three-parameter fit with spin-averaged scattering length and effective-range parameters $\bar{a}$ and $\bar{r}$ can reproduce the missing-mass spectrum but fails to describe simultaneously the total Λp cross-section data. Vice versa deducing $\bar{a}$ and $\bar{r}$ from a fit to the total-cross-section data fails to describe the missing-mass spectrum. Also a combined three-parameter fit of the missing-mass spectrum and the total Λp cross-section data fails to reproduce simultaneously both data sets with spin-averaged parameters $\bar{a}$ and $\bar{r}$.

Therefore, the singlet and triplet scattering lengths and effective ranges a_s, r_s, a_t, r_t are fitted as separate free parameters. Taking $|\mathcal{M}_s|^2$ as free parameter and the ratio $|\mathcal{M}_t|^2/|\mathcal{M}_s|^2$ as fixed parameter both the missing-mass spectrum and the total-cross-section data are perfectly reproduced in five-parameter fits. The ratio $|\mathcal{M}_t|^2/|\mathcal{M}_s|^2$ was varied over a wide range of values and important constraints on the parameters a_s, r_s, a_t, r_t were deduced. These are indicated in fig. 6 as experimentally allowed regions.

A characteristic feature of the best-fit solutions is the fact that the Λp FSI in the reaction $pp \to K^+\Lambda p$ is dominated by the singlet contribution. Another important result follows from a comparison of the singlet and triplet scattering lengths. The fact that $-a_s > -a_t$ means that the Λp interaction is more attractive in the singlet state than in the triplet state. This result is in accordance with the expectation deduced from an analysis of the binding energies of light hypernuclei [1].

Though the χ^2 values are only weakly dependent on $|\mathcal{M}_t|^2/|\mathcal{M}_s|^2$, ratios with $|\mathcal{M}_t|^2/|\mathcal{M}_s|^2 > 8$ can be excluded on the basis of the χ^2 criterion. In this context it is interesting to note that the fit yields for $|\mathcal{M}_t|^2/|\mathcal{M}_s|^2 > 1$ abnormally small singlet and large triplet effective ranges, $r_s < 1$ fm and $r_t > 6$ fm. Taking the definition of the effective range as interaction range such values are questionable. However, this problem can only be decided by experiments which allow to determine separately the absolute values of the singlet and triplet production matrix elements.

Most previous experiments provide only informations on the spin-averaged parameters $\bar{a}$ and $\bar{r}$ and the deduced values are given without errors estimates. But since the concept of spin-averaged parameters fails to describe simultaneously the $pp \to K^+X$ FSI enhancement and the Λp total cross-sections, we do not compare our spin-averaged parameters with previous determinations of $\bar{a}$ and $\bar{r}$. In this context we mention the general problem of defining spin-averaged parameters if singlet and triplet parameters are different.

Inspecting the world data set there is one experiment which provides direct information on the triplet

parameters a_t and r_t. The data on the Λp production in the reaction $K^- d \to \pi^- \Lambda p$ [7] show a marked FSI enhancement near the Λp threshold. Tai Ho Tan deduced a_t and r_t assuming that the $K^- d$ capture at rest occurs mainly from S-wave orbital admixtures. Spin and parity considerations imply that the final Λp state has spin one as the deuteron. Assuming that the FSI amplitude near threshold is dominated by the S-wave contribution, *i.e.* the $^3S_1$-state, the triplet scattering length and effective-range parameter a_t and r_t can directly be extracted from those data. The deduced values $a_t = -2.0 \pm 0.5$ fm and $r_t = 3.0 \pm 1.0$ fm [7] agree within one standard deviation with the experimentally allowed region of (a_t, r_t). They favor our five-parameter solutions for small ratios $|\mathcal{M}_t|^2/|\mathcal{M}_s|^2$. It should be mentioned that a re-analysis of the $K^- d \to \pi^- \Lambda p$ data is highly wanted in view of the importance and the high quality of those data.

The meson theoretical model predictions of the scattering lengths and effective ranges were compared with the experimentally allowed regions of (a_s, r_s) and (a_t, r_t) deduced from five-parameter fits of the data. In most cases the predicted singlet scattering lengths are too small and the triplet scattering lengths are too large. Only one model prediction is in agreement with the constraints deduced from the data. This finding was confirmed by a more direct test of the model predictions. The test was performed by keeping the predicted parameters in the fit routine fixed and fitting only $|M_s|^2$ and $|M_t|^2$. With one exception the model predictions fail to reproduce simultaneously the missing-mass spectrum near the Λp threshold and the total Λp cross-section data.

It should be emphasized that the shape of the FSI enhancement near the Λp threshold is the essential experimental information in order to evaluate the FSI parameters from the reaction $pp \to K^+ \Lambda p$. Since the most important part of the FSI enhancement is located in the sharply rising part of the missing-mass spectrum a high missing-mass resolution and sufficient statistical accuracy are needed. The effective missing-mass resolution of the SATURNE experiment [13] corresponded to a 1σ width of 2 MeV. Improving this value by an order of magnitude would allow to study the Λp FSI near $q = 0$ with higher accuracy. But not only the improvement of precision but also a systematic check of the method are important. An essential assumption of the factorization ansatz (eq. (3)) is that the production matrix element is constant, *i.e.* does not depend on the internal energy of the Λp final state. A direct check is to measure the reaction $pp \to K^+ \Lambda p$ at different energies and angles.

Ultimately, measurements with polarized beams and polarized targets are needed in order to disentangle the spin singlet and triplet contributions in the $pp \to K^+ \Lambda p$ reaction. Such measurements would allow to determine separately the singlet and triplet scattering lengths and effective ranges. The feasibility depends not only on the polarization of beam and target but also on the effective missing-mass resolution and luminosity.

We appreciate discussions with J. Haidenbauer, C. Hanhart and H. Rohdjeß. During the preparation of the paper we were informed about a theoretical study [37] of the $pp \to K^+ \Lambda p$ reaction using dispersion relations.

References

1. R.H. Dalitz, *Nuclear Interactions of the Hyperons* (Oxford University Press, Oxford, 1965).
2. R.H. Dalitz, Nucl. Phys. A **354**, 101c (1981).
3. C.B. Dover, A. Gal, Prog. Part. Nucl. Phys. **12**, 171 (1984).
4. G. Alexander *et al.*, Phys. Rev. **173**, 1452 (1968).
5. B. Sechi-Zorn *et al.*, Phys. Rev. **175**, 1735 (1968).
6. G. Alexander, *Proceedings of the International Conference on Hypernuclei* (Argonne National Laboratory, 1969).
7. Tai Ho Tan, Phys. Rev. Lett. **23**, 395 (1969).
8. C. Pigot *et al.*, Nucl. Phys. B **249**, 172 (1985).
9. H. Piekarz, Nucl. Phys. A **479**, 263c (1988).
10. A.C. Melissinos *et al.*, Phys. Rev. Lett. **14**, 604 (1965).
11. J.T. Reed *et al.*, Phys. Rev. **168**, 1495 (1968).
12. W.J. Hogan, P.A. Piroue, A.J.S. Smith, Phys. Rev. **166**, 1472 (1968).
13. R. Siebert *et al.*, Nucl. Phys. A **567**, 819 (1994).
14. J.T. Balewski *et al.*, Eur. Phys. J. A **2**, 99 (1998).
15. B. Bilger *et al.*, Phys. Lett. B **420**, 217 (1998).
16. M. Maggiora *et al.*, Nucl. Phys. A **691**, 329c (2001).
17. M.M. Nagels, T.A. Rijken, J.J. de Swart, Phys. Rev. D **15**, 2547 (1977).
18. M.M. Nagels, T.A. Rijken, J.J. de Swart, Phys. Rev. D **20**, 1633 (1979).
19. P.M.M. Maessen, T.A. Rijken, J.J. de Swart, Phys. Rev. C **40**, 226 (1989).
20. V.C.J. Stoks, Th.A. Riken, Phys. Rev. C **59**, 3009 (1999).
21. B. Holzenkamp, K. Holinde, J. Speth, Nucl. Phys. A **500**, 485 (1989).
22. A. Reuber, K. Holinde, J. Speth, Nucl. Phys. A **570**, 543 (1994).
23. J. Haidenbauer, W. Melnitchouk, J. Speth, AIP Conf. Proc. **603**, 421 (2001), nucl-th/0108062.
24. A. Deloff, Nucl. Phys. A **505**, 583 (1989).
25. J.M. Laget, Phys. Lett. B **259**, 24 (1991).
26. A. Sibirtsev, Phys. Lett. B **359**, 29 (1995).
27. G. Fäldt, C. Wilkin, Z. Phys. A **357**, 241 (1997).
28. A. Sibirtsev, W. Cassing, nucl-th/9802025 (1998).
29. A. Sibirtsev, K. Tsushima, A.W. Thomas, Phys. Lett. B **421**, 59 (1998)
30. K. Tsushima, A. Sibirtsev, A.W. Thomas, Phys. Rev. C **59**, 369 (1999).
31. A. Sibirtsev, K. Tsushima, W. Cassing, A.W. Thomas, Nucl. Phys. A **646**, 427 (1999)
32. R. Shyam, Phys. Rev. C **60**, 055213 (1999).
33. A. Gasparian, J. Haidenbauer, C. Hanhart, L. Kondratyuk, J. Speth, Phys. Lett. B **480**, 273 (2000)
34. N.G. Kelkar, B.K. Jain, Int J. Mod. Phys. E **9**, 431 (2000).
35. R. Shyam, G. Penner, U. Mosel, Phys. Rev. C **63**, 022202 (2001).
36. A. Gasparian, J. Haidenbauer, C. Hanhart, L. Kondratyuk, J. Speth, Nucl. Phys. A **684**, 397 (2001).
37. A. Gasparyan, J. Haidenbauer, C. Hanhart, J. Speth, Phys. Rev. C **69**. 034006 (2004), hep-ph/0311116.
38. K.M. Watson, Phys. Rev. **88**, 1163 (1952).
39. A.B. Migdal, Sov. Phys. JETP **1**, 2 (1955).

40. M.L. Goldberger, K.M. Watson, *Collision Theory* (J. Wiley, New York, 1964) p. 549.
41. J. Gillespie, *Final-State Interactions*, edited by K.M. Watson, Holden-Day Adv. Phys. Monographs (Holden-Day, San Francisco, London, Amsterdam, 1964).
42. R. Jost, Helv. Phys. Acta **20**, 356 (1947).
43. R. Jost, W. Kohn, Phys. Rev. **87**, 977 (1952).
44. V. Bargmann, Phys. Rev. **75**, 301 (1949).
45. V. Bargmann, Rev. Mod. Phys. **21**, 488 (1949).
46. J.S. Schwinger, Phys. Rev. **72**, 742 (1947).
47. H.A. Bethe, Phys. Rev. **76**, 38 (1949).
48. J.M. Blatt, V. Weisskopf, *Theoretical Nuclear Physics* (J. Wiley, New York, London, 1954).
49. E. Byckling, K. Kajantie, *Particle Kinematics* (J. Wiley, New York, London, 1973).
50. Particle Data Group, Eur. Phys. J. C **3**, 1 (1998).
51. F. James, M. Roos, Comput. Phys. Commun. **10**, 343 (1975).